Drug Delivery

DOI: 10.1002/ange.201002639

Intracellular pH-Responsive Mesoporous Silica Nanoparticles for the Controlled Release of Anticancer Chemotherapeutics**

*Chia-Hung Lee, Shih-Hsun Cheng, I-Ping Huang, Jeffrey S. Souris, Chung-Shi Yang, Chung-Yuan Mou, and Leu-Wei Lo**

Diseases of the liver pose a major healthcare challenge. Liver-related diseases, such as hepatitis, fatty liver, cirrhosis, and liver cancer, could be more effectively treated if the therapeutic drugs concentrate intracellularly within diseased tissue. Recently, we described the biodistribution of fluorescently labeled mesoporous silica nanoparticles (MSNs) in nude mice using non-invasive optical imaging techniques.[1] These studies indicated that even untargeted MSNs tend to rapidly accumulate in the liver simply by virtue of their size, surface charge, and topology. MSNs might thus afford a convenient, non-toxic means of treating many liver maladies. Indeed, MSNs have recently garnered considerable interest as drug carriers for the controlled release of therapeutics owing to their intrinsically large surface areas, large accessible pore volumes, highly ordered pore structures, and adjustable pore size.[2–8] Furthermore, the abundant silanol groups (Si–OH) that tile their pore surfaces facilitate MSN post-synthesis modification with various organic linkers, thereby simplifying the design of controlled-release mechanisms for drug delivery.[9] MSNs, with diameters between 50 nm and 100 nm, readily undergo endocytosis in vivo with much higher cellular uptake efficiency than the passive transfer and simple diffusion of free drug molecules across cell membranes.[2,5,10]

To enable regulated drug release, a variety of control mechanisms have been explored that include modulation of drug-platform coupling by external magnetic fields, near-infrared light, and radio-frequency (RF) heating.[11] Exploiting differences in pH is also a viable approach, such as the use of pH-sensitive polymers to release doxorubicin at endosomal pH values.[12–19] Based upon the conjugation of doxorubicin to a polymer backbone by active bonds, such as acetal,[20] hydrazone,[21,22] or ester bonds, this method addresses one of the principal limitations of conventionally administered doxorubicin in chemotherapy: its significant systemic toxicity. Unfortunately, it and most polymer nanoparticles are somewhat limited in their capacity to accommodate drugs. Although a number of studies have confirmed endosomal release of doxorubicin, considerable extracellular pre-release of the drug, from hydrolysis of the drug-conjugating linker by enzymatic catalysis, remains a problem.[23]

Unlike polymer nanoparticles, the silica frameworks that comprise MSNs are inherently immune to hydrolysis and enzymatic degradation, and enable extraordinarily large loadings of drugs. Moreover, the narrow confines of the MSN nanochannels provide a physical barrier to enzyme entry, as most enzymatic proteins have diameters considerably greater than those of the MSN pores. Therefore drugs conjugated to the inner walls of the MSN nanochannels are largely protected from in vivo hydrolysis and premature release.

Although enzymes cannot easily enter MSN nanochanels, the protons found within acidic endosomes and lysosomes can, thereby providing a means of cleaving the labile hydrazone bonds that link drugs to the nanochannel walls. Thus MSNs can exploit the enhanced permeability and retention (EPR) effect of tumor tissue to release highly toxic drugs within tumors, but with nearly none of the side effects that arise from premature drug release.[24] Moreover, the combination of the intrinsically large drug payload and typical endosomal proton densities of MSNs enables the localized, sustained release of drug molecules within diseased tissue. The conjugation of drugs to MSN nanochannel walls by pH-sensitive linkers further decreases systemic toxicity after tumor cell lysis by reducing fluctuations and peaks of unutilized drug in extracellular plasma.

Large-pore Atto-647-MSN samples, with a hexagonal well-ordered pore structure, were synthesized through sol–gel co-condensation of tetraethoxysilane (TEOS) and Atto-647-conjugated 3-aminopropyltrimethoxysilane (APTS) in the presence of a surfactant (CTAB), a swelling agent (n-octane),

[*] S.-H. Cheng,[+] I.-P. Huang, Prof. L.-W. Lo
Division of Medical Engineering Research
National Health Research Institutes
Zhunan Miaoli 350 (Taiwan)
Fax: (+886) 37-586-440
E-mail: lwlo@nhri.org.tw
Dr. C.-H. Lee,[+] Prof. C.-S. Yang
Center for Nanomedicine Research
National Health Research Institutes
Zhunan, Miaoli 350 (Taiwan)
Dr. J. S. Souris
Department of Radiology, The University of Chicago
Chicago, IL 60637 (USA)
Prof. C.-Y. Mou
Department of Chemistry, National Taiwan University
Taipei 106 (Taiwan)
S.-H. Cheng[+]
Institute of NanoEngineering and MicroSystems
National Tsing Hua University
Hsinchu 300 (Taiwan)
[+] These authors contributed equally to this work.

[**] This study was supported by the Grants MED-098-PP-04 and NM-098-PP-01 from the National Health Research Institutes of Taiwan; and NSC 098-2221-E-400-001 from the National Science Council of Taiwan. We thank Yu-Ching Chen, Chia-Hui Chu, and Dr. Ching-Mao Huang for their assistance with TEM and EDX measurements.

Supporting information for this article is available on the WWW under http://dx.doi.org/10.1002/anie.201002639.

and a base catalyst (NH_4OH). The incorporation of a near-infrared (NIR) fluorophore (Atto-647) within the MSN silica framework provided a means of non-invasively tracking the biodistribution in vivo, as most mammalian tissues are relatively transparent at NIR wavelengths, and background tissue autofluorescence is minimal.[1,25–27] After sol–gel co-condensation of Atto-647-APTS and TEOS, surfactant molecules were fully removed by extraction under an NH_4NO_3/alcohol solution to provide large surface areas for further conjugation with pH-sensitive linkers. The loading fraction of doxorubicin within MSNs was determined by measuring changes in optical absorption of the solution phase at 490 nm (Table 1).

Table 1: Loading percentages and isoelectric points of various Dox-conjugated MSN samples.

Sample	Dox loading [wt%]	Isoelectric point
MSN-hydrazone-Dox	1.09	3.69
TA-MSN-hydrazone-Dox	0.51	6.28
Atto-647-MSN-hydrazone-Dox	0.56	3.58

To enhance cellular uptake and minimize self-aggregation, the outermost surfaces of MSNs were modified with trimethylammonium (TA) groups that increase the nanoparticle surface charge (see zeta potential measurements in the Supporting Information, Figure S1). The loading percentage by weight of doxorubicin in MSN-hydrazone, TA-MSN-hydrazone, and Atto-647-MSN-hydrazone was 1.09, 0.51, and 0.56% respectively, with corresponding isoelectric points of 3.69, 6.28, and 3.58.

The pH-sensitive linker was conjugated onto MSN nanochannel surfaces by hydrazone bonds. First, the nanochannels of MSN were modified with aldehyde groups through the post-modification of the MSN inner surface with triethoxysilylbutyraldehyde. Next, the aldehyde group was reacted with one hydrazide group of adipic acid dihydrazide to produce a reactive hydrazone bond. Another hydrazide group was further reacted with the ketone groups of doxorubicin to produce additional hydrazone bonds in doxorubicin conjugation. The pH-sensitive linkers, when loaded with drug, possessed two hydrazone bonds that were cleavable at endosomal pHs.

Figure 1a shows MSN delivery of doxorubicin to a tumor, with cleavage taking place for local pH values between 4 and 6, corresponding to those found within endosomes and lysosomes. Through EPR effects, doxorubicin-loaded MSNs inherently accumulate in the solid tumors of liver, demonstrating substantial anticancer effects with human hepatoma cells (Hep-G2). TEM images of MSN-hydrazone-Dox (Figure 1b,c) show that MSN-hydrazone-Dox has generally hexagonal shapes and uniform sizes, with average particle diameters of about 100 nm. Using n-octane as a swelling agent to expand the inner micelle space, the as-synthesized MSNs possessed both large pore diameters (ca. 5.0 nm) and well-ordered pore structures (Figure 1c). Moreover, MSN mor-

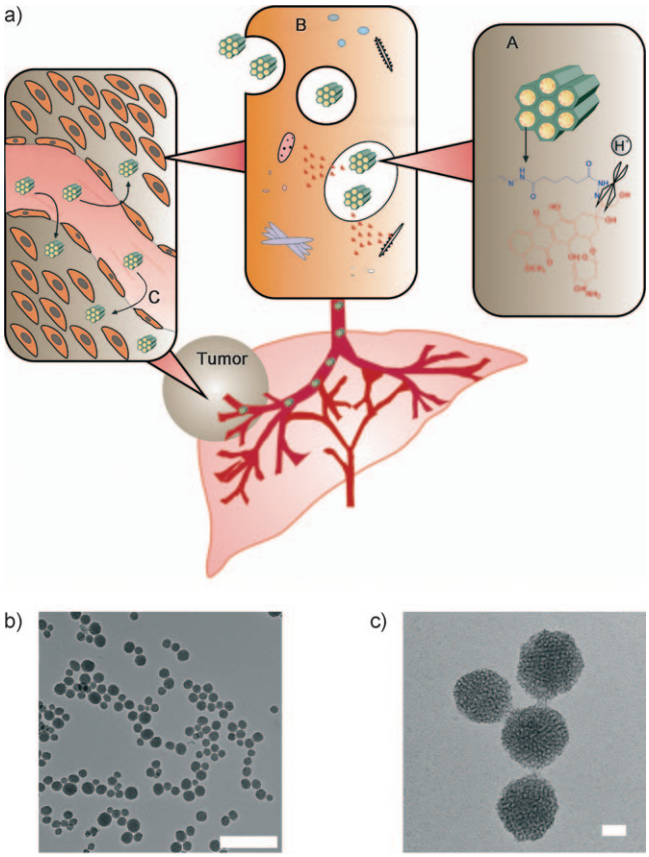

Figure 1. a) The pH-sensitive MSN drug delivery platform in the chemotherapeutic treatment of liver cancer. Nonspecific uptake of MSN-hydrazone-Dox from the blood stream (C) by the liver cancer cells occurs through endocytosis (A). Hydrolysis of hydrazone bond of the pH-sensitive linkers (B) in the acidic environment of endosomes/lysosomes (pH 5–6) releases doxorubicin (red) intracellularly from the MSN nanochannels. b,c) TEM images of the characteristic hexagonal structure of MSN-hydrazone-Dox. Scale bars: b) 500 nm, c) 20 nm.

phology and structure were not affected by the conjugation of hydrazone linkers and drug molecules onto the MSN surface. Nitrogen adsorption–desorption isotherms and pore-size distributions of MSN, MSN-aldehyde, and MSN-hydrazide are shown in the Supporting Information, Figure S2. The amount of nitrogen adsorbed gradually decreased from 1265 $m^2 g^{-1}$ for MSN to 823 $m^2 g^{-1}$ for MSN-aldehyde and to 614 $m^2 g^{-1}$ for MSN-hydrazide. At the same time, the pore volumes and pore diameter decreased from 1.675 $cm^3 g^{-1}$ and 5.2 nm for MSN to 0.935 $cm^3 g^{-1}$ and 4.7 nm for MSN-aldehyde and to 0.661 $cm^3 g^{-1}$ and 3.8 nm for MSN-hydrazide. Thus both the addition and the modification of the pH-sensitive linker were easily observed.

To characterize the chemical bonds and surface organic groups within our MSN samples and their post-synthesis modifications/conjugations, we employed FTIR spectroscopy (Supporting Information, Figure S3). The spectra of bare MSN show only the surface silanol groups and low-frequency silica vibrations. The C–H stretches at 2940 cm^{-1} and 2980 cm^{-1} appear only on surface-functionalized MSN samples. The aldehyde-modified MSN sample has a C=O stretch mode at about 1720 cm^{-1}. Conjugation of adipic acid dihy-

drazide and doxorubicin produced hydrazone and hydrazide bonds, as seen in the overlapping-absorption peaks of imine (C=N) and amide (C=O) at 1662 cm^{-1} and the N–H bending mode bands at about 1552 cm^{-1}. Other bands at 1400 cm^{-1} are attributed to CH_2 bends.

We also measured the FT-IR spectra of a TA-MSN sample and post-synthesis modifications/conjugations (Supporting Information, Figure S4). The TA groups are modifications of the original surfaces of MSNs by both C–H stretching bands at 2900 cm^{-1} and 2987 cm^{-1} and CH_2 bends at 1470 cm^{-1}. The additional conjugations of TA-MSN with aldehyde–silane, adipic acid dihydrazide, and doxorubicin were also characterized by FTIR spectroscopy, as was the conjugation of doxorubicin to the pH-sensitive linkers that tiled the MSN nanochannels by the formation of hydrazone bonds.

To verify the pH-sensitive release mechanism, we used fluorescence spectroscopy and imaging to quantitate the release of doxorubicin from Atto-647-MSN-hydrazone-Dox samples (Figure 2). After incubating Atto-647-MSN-hydrazone-Dox samples for different time periods and pH values, specimens were centrifuged and the resulting precipitate pellets and supernatant solutions were examined separately. As doxorubicin is itself weakly fluorescent, with absorption and emission spectra maxima distinct from those of Atto-647 (doxorubicin: λ_{ex} 440, λ_{em} 580 nm; Atto-647: λ_{ex} 620, λ_{em} 670 nm), and doxorubicin is optically scattering at higher densities, both white light and fluorescence images were made at corresponding spectral maxima (Figure 2). From white-light observations, clear supernatants and orange pellets were observed before (Figure 2 a1) and after (Figure 2 a2) six-hour incubation of Atto-647-MSN-hydrazone-Dox samples at pH 7.4. Incubation of the same specimens at pH 4.5 for six hours, however, resulted in cloudy orange supernatants (Figure 2 a3).

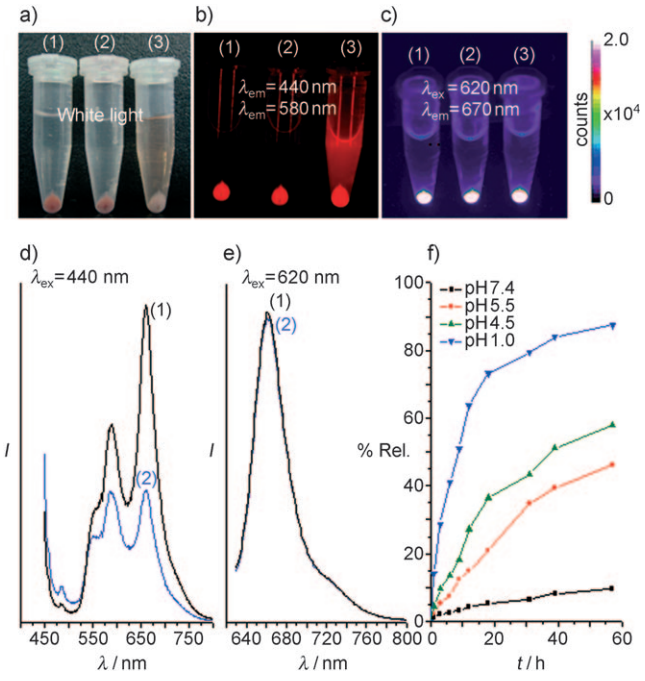

Figure 2. a) White-light and b,c) fluorescent images of the centrifuged MSN-hydrazone-Dox samples after incubation for different periods and pH values. 1) pH 7.4 0 h, 2) pH 7.4 6 h, 3) pH 4.5 6 h. d,e) Fluorescent spectra of Atto-647-MSN-hydrazone-Dox samples before (1) and after (2) incubation at pH 4.5 for 6 h. f) % Release profile of MSN-hydrazone-Dox for different pH values.

To verify that doxorubicin was being selectively released into the pH 4.5 buffer, we imaged the supernatant solution specimens for doxorubicin fluorescence. These studies confirmed that no discernable doxorubicin was released at neutral pH (Figure 2 b1,b2). At the endosomal pH of 4.5, however, quite a few doxorubicin molecules were cleaved from the MSN nanochannels (Figure 2 b3). To further substantiate that acidic pH values can only trigger the release of doxorubicin (Atto-647 can be stabilized within MSN against the leaching from endosome pHs), we also imaged the centrifugal samples with Atto-647 fluorescence, namely excitation at 620 nm. These studies confirmed that no Atto-647 was released either at neutral or acidic pH; only the MSN pellets fluoresced (Figure 2 c1–3).

We also recorded the fluorescence spectra of Atto-647-MSN-hydrazone-Dox samples before and after their incubation for various periods and pHs (Figure 2 d,e). When specimens were excited at the absorption maximum of doxorubicin (440 nm), two emission maxima were observed: one at 580 nm from doxorubicicn, and the other at 670 nm from Atto-647. Because the emission spectra of doxorubicin ($\lambda_{em.}$ = 580 nm–640 nm) overlapped the absorption spectra of Atto-647 (λ_{ex} = 600 nm–650 nm), and as the average distance between donor and acceptor was shorter than 10 nm, efficient FRET took place prior to the release of doxorubicin from Atto-647-MSN (Figure 2 d1). In comparison, following release of doxorubicin from the nanoparticles at pH 4.5, the emission spectra of specimens excited at 440 nm indicated the decrease of fluorescence intensity of both doxorubicin and Atto-647 (Figure 2 d2), which was due to the decrease of doxorubicin concentration serving as FRET donor at pH 4.5. Excitation of Atto-647-MSN-hydrazone-Dox samples at 620 nm, the peak absorption wavelength of Atto-647, yielded no measurable differences between pre- and post-release of doxorubicin in the fluorescent emission of Atto-647-MSN (Figure 2 e). This result provided evidence for the high stability of co-condensed Atto-647 in MSN at different pH values and suggested the decrease of FRET efficiency at pH 4.5 was due to the release of doxorubicin but Atto-647.

To characterize the functionality of the pH-sensitive linker release of doxorubicin, MSN-hydrazone-Dox samples were incubated at pH values of 7.4, 5.5, 4.5, and 1.0, and the released amounts were determined by optical absorbance measurements of the solution phase at 440 nm. From these releasing-profile studies (Figure 2 f), we determined that nanoparticle release of doxorubicin was both time- and pH-dependent, with almost no release under normal physiological conditions (that is, at pH 7.4). Release rates of doxorubicin (slopes of curves in Figure 2 f) show increased sustained rates for increased acidities, with approximately 80 %, 40 %, and 30 % of the drug released within 24 hours at pH 1.0, 4.5, and 5.5, respectively. As such, these findings

strongly suggest that the nanochannels of MSN had no affect on either protons entering or of doxorubicin excitation; pH-responsive MSN had in increased doxorubicin release rate over the 60 hour period in mimicked environments of late-endosome and lysosome, where the pHs are in the range 5.0–6.0.

To verify that MSN-hydrazone-Dox could enter the cells through endocytosis and accumulate within endosomes and lysosomes, we used confocal microscopy to characterize cellular uptake of Atto-647-labeled MSN-hydrazone-Dox (Figure 3a–c). The addition of Atto-647-MSN-hydrazone-Dox to Hep-G2 cells, endosomes, and lysosomes were labeled with green fluorescent lysotracker (Figure 3b). After 2 hours of incubation, the red fluorescence of Atto-647-MSN-hydrazone-Dox was readily apparent within Hep-G2 cells (red in Figure 3a) and co-localized with lysotracker green fluorescence (green in Figure 3b, yellow in Figure 3c), thus indicating that the Atto-647-MSN-hydrazone-Dox had become highly concentrated within endosomes and lysosomes of the Hep-G2 cell.

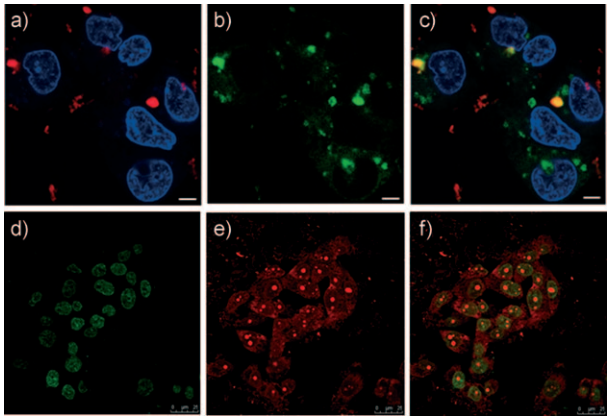

Figure 3. a) Confocal microscopy of the cellular uptake behavior of Atto-647-MSN-hydrazone-Dox (MSN: red fluorescence of Atto-647; nuclei: blue fluorescence of Hoechst 33342 staining); b) Hep-G2 cells labeled with lysotracker to mark lysosomes (green); c) merging of images (a) and (b). To identify apoptotic responses, Hep-G2 cells were pre-treated with Atto-647-MSN-hydrazone-Dox for 24 h. d) TUNEL assay from fluorescein labeling (green); e) chromosomes stained with propidium iodide (red fluorescence); f) merging of images (d) and (e).

Although mechanism of action for doxorubicin is not known, it is believed to inhibit the action of topoisomerase II or intercalate DNA strands, leading to DNA double-strand breaks and inhibition of DNA replication and transcription.[28,29] To further assess the MSN release of doxorubicin, the endosomal escape of the drug, and its effect on cell viability, we employed TUNEL (terminal deoxynucleotidyl transferase dUTP nick-end labeling) assays to detect DNA strand breaks (Figure 3d). By fluorescein labeling of the terminal ends of nucleic acids, TUNEL assays enable highly efficient optical detection of the DNA fragmentation that results from cell apoptosis. As shown in Figure 3e, Hep-G2 chromosomes stained with propidium iodide (red fluorescence) co-localized nicely with TUNEL images of DNA fragmentation in Hep-G2 nuclei (Figure 3f).

To further provide the physical evidence for subcelluar residence of nanoparticles, TEM was applied to image the cell uptake of MSN-hydrazone-Dox and its sequestration within late endosomes and lysosomes (Figure 4a,b). The compositional analysis of cell sections was measured simultaneously using energy-dispersive X-ray spectroscopy (EDX; Figure 4c,d). The composition spectrum of selected endosome/lysosome containing MSN-hydrazone-Dox showed the clear presence of silicon (Figure 4d), in contrast to that of the other subcellular domains, where no silicon was observed (Figure 4c).

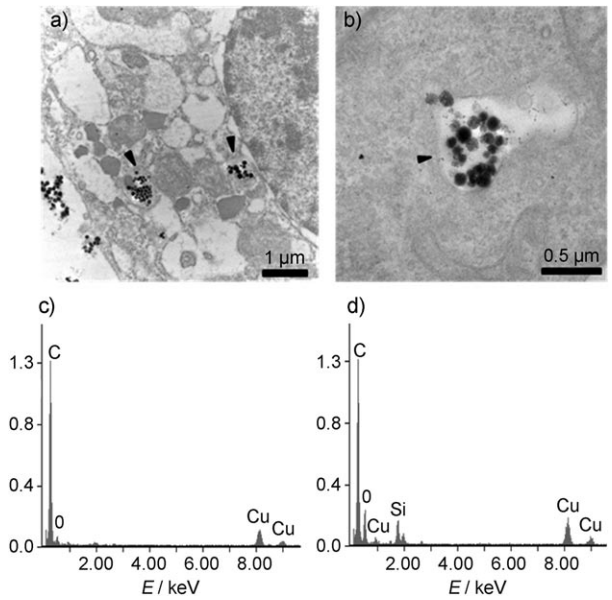

Figure 4. a) TEM imaging of the cell uptake of MSN-hydrazone-Dox and its accumulation within endosomes and lysosomes (black arrows); b) enlarged view; c,d) EDX measurement of subcellular area in the absence of MSN-hydrazone-Dox (c) and selected endosome/lysosome-containing MSN-hydrazone-Dox (d).

To evaluate the cytotoxicity of MSN-hydrazone-Dox, a 3-(4,5-dimethylthiazol-2-y1)-2,5-diphenyltetrazolium bromide (MTT) assay was employed to assess the cell viability. Under normal physiological pH conditions (i.e., at pH 7.4), release-profile studies indicated a very slow and less than 10% release of doxorubicin over 60 hour time period (Figure 2f). To assess the cytotoxicity of the minute released doxorubicin at pH 7.4, we further treated Hep-G2 cells with free doxorubicin at concentrations corresponding to 2%, 5%, 8%, and 10% of that in MSN-hydrazone-Dox; the MTT assays showed negligible cytotoxicity under these conditions (Figure 5a). On the contrary, with Hep-G2 cells incubated with 100 g TA-MSN-hydrazone-Dox, the cell viability was reduced to about 30%. It could be reversed if co-treating cells with 1 μM bafilomycin A1 (BA) (Figure 5b). BA is known as a strong inhibitor of the vacuolar type H^+-ATPase.[30] It can increase the endosomal/lysosomal pH, and thus can impede

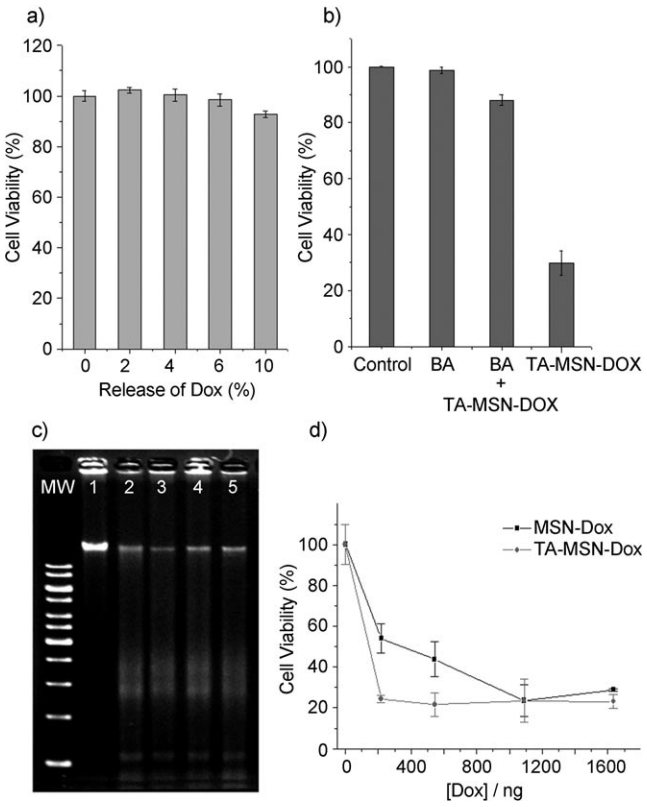

Figure 5. a) Cell viability studies with MTT assays of Hep-G2 cells treated with free doxorubicin at concentrations corresponding to 2%, 5%, 8%, and 10% of that in MSN-hydrazone-Dox. b) Endosomal/lysosomal pH effects on TA-MSN-hydrazone-Dox-induced cytotoxicity. Hep-G2 cells were co-treated with TA-MSN-hydrazone-Dox and 1 μM bafilomycin A1 (BA), a proton pump inhibitor. c) Fragmentation effects of MSN-hydrazone-Dox on Hep-G2 chromosomal DNA after incubation for 24 h. Lane 1: doxorubicin-free control, lane 2: free doxorubicin, lane 3: MSN-hydrazone-Dox, lane 4: TA-MSN-hydrazone-Dox, lane 5: Atto-647-MSN- hydrazone-Dox. d) MTT Hep-G2 cell viability assay of MSN-hydrazone-Dox and TA-MSN-hydrazone-Dox after incubation for 24 h.

the release of doxorubicin from the TA-MSN-hydrazone-Dox sequestered in endosome/lysome.

The effectiveness of free and MSN-conjugated doxorubicin was also confirmed by DNA fragmentation studies. Hep-G2 cells were incubated with either 5 $\mu g\,mL^{-1}$ free or 0.55 $\mu g\,mL^{-1}$ MSN-conjugated doxorubicin for 24 hours, DNA ladders were applied to 1.5% agarose gels for electrophoretic comparison of doxorubicin-induced DNA fragmentation (Figure 5c). As can be seen from lanes 2 and 2–5 of Figure 5c, free doxorubicin at concentrations 10 times higher (5 $\mu g\,mL^{-1}$) than those typically released intracellularly at endosomal pH by MSN-hydrazone-Dox specimens (0.55 $\mu g\,mL^{-1}$) were required to have comparable levels of apoptosis. Thus the in vitro performance of the MSN platform was ten times more efficient than the use of free drug alone, with minimal un-utilized drug released.

With Hep-G2 cells incubated with MSN-hydrazone-Dox and TA-MSN-hydrazone-Dox nanoparticles with various concentrations of Dox loading for 24 hours, MTT analyses (Figure 5d) showed that TA-MSN-hydrazone-Dox samples had higher anticancer activities than MSN-hydrazone-Dox samples. The more positively charged surfaces of TA-modified MSNs increase the efficiency of their uptake by cells. Thus the release of only 200 ng of doxorubicin (corresponding to a total release of doxorubicin) from TA-MSN-hydrazone-Dox resulted in rapid decline of cell viability to about 20%. Therefore, surface charge manipulation of MSNs by the incorporation of positively charged TA groups directly correlated with cytotoxicity.

To observe the biodistribution of Atto-647-MSN-hydrazone-Dox in mice, organs were imaged ex vivo using a custom-built optical imaging system previously described.[1] Three hours following intravenous injection of 16 $mg\,kg^{-1}$ Atto-647-MSN-hydrazone-Dox into mice, major organs were obtained. Visceral group fluorescence imaging of the organs revealed that the overwhelming majority of Atto-647-MSN-hydrazone-Dox resided within the liver (Figure 6a,b).

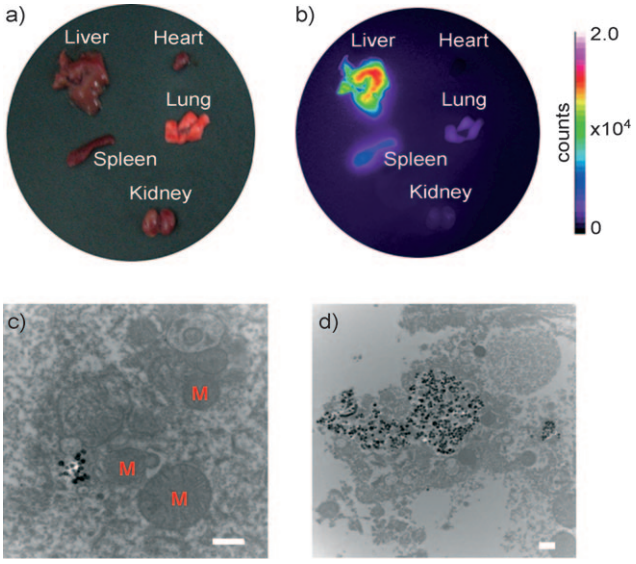

Figure 6. Organs from a mouse dissected 3 h after intravenous injection of Atto-647-MSN-hydrazone-Dox. a) Representative white-light and b) NIR fluorescent images of the organs; c) TEM images of a 70 nm-thick section of liver viscerated from an anesthetized mouse 3 h after intravenous injection of Atto-647-MSN-hydrazone-Dox. (Scale bars 500 nm; M = mitochondria.)

Confirmation of tissue uptake was provided by TEM images of frozen tissue cross-sections obtained three hours after injection of Atto-647-MSN-hydrazone-Dox. As indicated previously by fluorescence imaging, TEM imaging of tissue sections demonstrated substantial and preferential hepatic uptake of nanoparticles (Figure 6d), with MSNs being concentrated within intracellular vesicles and surrounded by mitochondria (Figure 6c). Evidence of doxorubicin-induced apoptosis can be seen in Figure 6d, with a number of hepatic cells being fractured and the presence of numerous vacuoles.

In summary, our pH-sensitive drug release mechanism demonstrated highly efficient operation in vitro at endosomal and lysosomal pHs. With the drug-loaded release mechanism

incorporated into the nanochannels of MSNs, the resulting drug delivery platform offers a number of attractive features: 1) sustained and proportionate release of potentially toxic drugs, 2) decreased non-specific release from enzymatic hydrolysis, (3) increased cell uptake through easily modified surface charge, and 4) increased drug loading and release efficiency. Thus drugs with toxicities those are currently dose-limiting, such as the use of doxorubicin in chemotherapy, can be administered with significantly reduced systemic side-effects compared to traditional treatments. The intrinsic accumulation of MSNs in the liver, its susceptibility to rapid endocytosis, and the observed sustained release of drug payload, minimizes systemic toxicity and greatly facilitates the treatment of hepatic disease. Although EPR effects in themselves enable a measure of tumor targeting, outermost surface funtionalization of MSNs with receptor-specific ligands (for example folic acid or RGD peptide) would further enhance the platform's therapeutic profile by actively targeting the pathology and simultaneously lessen collateral damage. Moreover, apart from to doxorubicin, the pH-sensitive drug release mechanism can no doubt be applied to other anticancer drugs that possess functional ketones or aldehydes, such as cerubidine (daunorubicin chloride) and idarubicin, which is an anthracycline antileukemic drug used as a first line treatment of acute myeloid leukemia.

Received: May 2, 2010
Published online: September 23, 2010

Keywords: antitumor agents · apoptosis · controlled release · doxorubicin · mesoporous silica

[1] C. H. Lee, S. H. Cheng, Y. J. Wang, Y. C. Chen, N. T. Chen, J. Souris, C. T. Chen, C. Y. Mou, C. S. Yang, L. W. Lo, *Adv. Funct. Mater.* **2009**, *19*, 215.

[2] a) I. I. Slowing, J. L. Vivero-Escoto, C. W. Wu, V. S. Lin, *Adv. Drug Delivery Rev.* **2008**, *60*, 1278; b) B. G. Trewyn, I. I. Slowing, S. Giri, H. T. Chen, V. S. Lin, *Acc. Chem. Res.* **2007**, *40*, 846.

[3] M. Liong, S. Angelos, E. Choi, K. Patel, J. F. Stoddart, J. I. Zink, *J. Mater. Chem.* **2009**, *19*, 6251.

[4] a) M. Vallet-Regí, F. Balas, D. Arcos, *Angew. Chem.* **2007**, *119*, 7692; *Angew. Chem. Int. Ed.* **2007**, *46*, 7548; b) M. Vallet-Regi, A. Ramila, R. P. del Real, J. Perez-Pariente, *Chem. Mater.* **2001**, *13*, 308; c) R. Mortera, S. Fiorilli, E. Garrone, E. Verne, B. Onidab, *Chem. Eng. J.* **2010**, *156*, 184; d) R. Mellaerts, J. A. G. Jammaer, M. Van Speybroeck, H. Chen, J. Van Humbeeck, P. Augustijns, G. Van den Mooter, J. A. Martens, *Langmuir* **2008**, *24*, 8651.

[5] W. H. Suha, Y.-H. Suhb, G. D. Stuckya, *Nano Today* **2009**, *4*, 27.

[6] a) J. K. Hsiao, C. P. Tsai, T. H. Chung, Y. Hung, M. Yao, H. M. Liu, C. Y. Mou, C. S. Yang, Y. C. Chen, D. M. Huang, *Small* **2008**, *4*, 1445; b) H. M. Liu, S. H. Wu, C. W. Lu, M. Yao, J. K. Hsiao, Y. Hung, Y. S. Lin, C. Y. Mou, C. S. Yang, D. M. Huang, Y. C. Chen, *Small* **2008**, *4*, 619; c) F. Lu, S. H. Wu, Y. Hung, C. Y. Mou, *Small* **2009**, *5*, 1408; d) S. H. Wu, Y. S. Lin, Y. Hung, Y. H. Chou, Y. H. Hsu, C. Chang, C. Y. Mou, *ChemBioChem* **2008**, *9*, 53.

[7] a) P. P. Yang, Z. W. Quan, Z. Y. Hou, C. X. Li, X. J. Kang, Z. Y. Cheng, J. Lin, *Biomaterials* **2009**, *30*, 4786; b) C.-L. Zhu, X.-Y. Song, W.-H. Zhou, H.-H. Yang, Y.-H. Wen, X.-R. Wang, *J. Mater. Chem.* **2009**, *19*, 7765; c) G. Wang, A. N. Otuonye, E. A. Blair, K. Denton, Z. Tao, T. Asefa, *J. Solid State Chem.* **2009**, *182*, 1649; d) P. P. Yang, Z. W. Quan, L. L. Lu, S. S. Huang, J. Lin, *Biomaterials* **2008**, *29*, 692.

[8] a) M. Kilpeläinen, J. Riikonen, M. A. Vlasova, A. Huotari, V. P. Lehto, J. Salonen, K. H. Herzig, K. Jarvinen, *J. Controlled Release* **2009**, *137*, 166; b) T. Lebold, C. Jung, J. Michaelis, C. Brauchle, *Nano Lett.* **2009**, *9*, 2877; c) G. Sun, Y. Chang, S. Li, Q. Li, R. Xu, J. Gua, E. Wang, *Dalton Trans.* **2009**, 4481.

[9] a) S. Angelos, Y. W. Yang, K. Patel, J. F. Stoddart, J. I. Zink, *Angew. Chem.* **2008**, *120*, 2254; *Angew. Chem. Int. Ed.* **2008**, *47*, 2222; b) A. Schlossbauer, J. Kecht, T. Bein, *Angew. Chem.* **2009**, *121*, 3138; *Angew. Chem. Int. Ed.* **2009**, *48*, 3092; c) A. Bernardos, E. Aznar, C. Coll, R. M. -Manez, J. M. Barat, Ma. D. Marcos, F. Sancenon, A. Benito, J. Soto, *J. Controlled Release* **2008**, *131*, 181; d) A. Bernardos, E. Aznar, M. D. Marcos, R. M. -Manez, F. Sancenon, J. Soto, J. M. Barat, P. Amoros, *Angew. Chem.* **2009**, *121*, 5998; *Angew. Chem. Int. Ed.* **2009**, *48*, 5884; e) V. Cauda, L. Muhlstein, B. Onida, T. Bein, *Microporous Mesoporous Mater.* **2009**, *118*, 435.

[10] C. Gao, I. Izquierdo-Barba, I. Nakase, S. Futaki, J. Ruan, K. Sakamoto, Y. Sakamoto, K. Kuroda, O. Terasaki, S. Che, *Microporous Mesoporous Mater.* **2009**, *122*, 201.

[11] a) J. Lu, E. Choi, F. Tamanoi, J. I. Zink, *Small* **2008**, *4*, 421; b) C. Liu, J. Guo, W. Yang, J. Hu, C. Wang, S. Fu, *J. Mater. Chem.* **2009**, *19*, 4764.

[12] a) S. Angelos, N. M. Khashab, Y. W. Yang, A. Trabolsi, H. A. Khatib, J. F. Stoddart, J. I. Zink, *J. Am. Chem. Soc.* **2009**, *131*, 12912; b) L. Du, S. Liao, H. A. Khatib, J. F. Stoddart, J. I. Zink, *J. Am. Chem. Soc.* **2009**, *131*, 15136.

[13] a) T. R. Kyriakides, C. Y. Cheung, N. Murthy, P. Bornstein, P. S. Stayton, A. S. Hoffman, *J. Controlled Release* **2002**, *78*, 295; b) S.-W. Song, K. Hidajat, S. Kawi, *Chem. Commun.* **2007**, 4396.

[14] A. A. Attama, U. F. Ezeamama, *Drug Delivery* **2005**, *12*, 103.

[15] K. Na, *Korean J. Gastroenterol.* **2007**, *49*, 314.

[16] E. S. Lee, K. Na, Y. H. Bae, *J. Controlled Release* **2005**, *103*, 405.

[17] A. Corma, U. Diaz, M. Arrrica , E. Fernandez, I. Ortega, *Angew. Chem.* **2009**, *121*, 6365; *Angew. Chem. Int. Ed.* **2009**, *48*, 6247.

[18] a) C.-Y. Hong, X. Li, C.-Y. Pan, *J. Mater. Chem.* **2009**, *19*, 5155; b) J. W. Liu, X. M. Jiang, C. Ashley, C. J. Brinker, *J. Am. Chem. Soc.* **2009**, *131*, 7567; c) H. Lin, G. Zhu, J. Xing, B. Gao, S. Qiu, *Langmuir* **2009**, *25*, 10159.

[19] a) Q. Gao, Y. Xu, D. Wu, Y. Sun, X. Li, *J. Phys. Chem. C* **2009**, *113*, 12753; b) W. Xu, Q. Gao, Y. Xu, D. Wua, Y. Sun, *Mater. Res. Bull.* **2009**, *44*, 606.

[20] E. R. Gillies, A. P. Goodwin, J. M. J. Frechet, *Bioconjugate Chem.* **2004**, *15*, 1254.

[21] Y. Bae, N. Nishiyama, K. Kataoka, *Bioconjugate Chem.* **2007**, *18*, 1131.

[22] T. Etrych, P. Chytil, M. Jelinkova, B. Rihova, K. Ulbrich, *Macromol. Biosci.* **2002**, *2*, 43.

[23] M. A. Yessine, J. C. Leroux, *Adv. Drug Delivery Rev.* **2004**, *56*, 999.

[24] B. Thierry, *Curr. Drug Delivery* **2009**, *6*, 391.

[25] P. P. Ghoroghchian, P. R. Frail, K. Susumu, D. Blessington, A. K. Brannan, F. S. Bates, B. Chance, D. A. Hammer, M. J. Therien, *Proc. Natl. Acad. Sci. USA* **2005**, *102*, 2922.

[26] E. I. Altinoglu, T. J. Russin, J. M. Kaiser, B. M. Barth, P. C. Eklund, M. Kester, J. H. Adair, *ACS Nano* **2008**, *2*, 2075.

[27] S. B. Lee, M. Hassan, R. Fisher, O. Chertov, V. Chernomordik, G. Kramer-Marek, A. Gandjbakhche, J. Capala, *Clin. Cancer Res.* **2008**, *14*, 3840.

[28] A. Bodley, L. F. Liu, M. Israel, R. Seshadri, Y. Koseki, F. C. Giuliani, S. Kirschenbaum, R. Silber, M. Potmesil, *Cancer Res.* **1989**, *49*, 5969.

[29] C. Ramachandran, T. S. Samy, X. L. Huang, Z. K. Yuan, A. Krishan, *Biochem. Pharmacol.* **1993**, *45*, 1367.

[30] T. Yoshimori, A. Yamamoto, Y. Moriyama, M. Futai, Y. Tashiro, *J. Biol. Chem.* **1991**, *266*, 17707.

